Astron. Astrophys. 300, 65-77 (1995)

ASTRONOMY AND ASTROPHYSICS

The three rings of the isolated galaxy NGC 7217

L. Verdes-Montenegro[1,2], **A. Bosma**[1], **and E. Athanassoula**[1]

[1] Observatoire de Marseille, 2 Place le Verrier, F-13248 Marseille Cedex 4, France
[2] Instituto de Astrofísica de Andalucía, CSIC, Apdo. Correos 3004, E-18080 Granada, Spain

Received 15 June 1994 / Accepted 21 November 1994

Abstract. We present WSRT H I line observations, together with CCD-$BVRI$ photometry, of NGC 7217, which is known to be an isolated galaxy with an inner ring, an inner pseudoring and an outer ring, but for which no clear bi-symmetric distortion is immeadiately apparent.

Assuming, as is known to be the case for barred galaxies, that the outer ring corresponds to the outer Lindblad resonance, we have derived the expected locations for the other resonances using a combined optical/H I rotation curve. Our result is that the observed inner ring coincides with the inner Lindblad resonance and the inner pseudoring with the ultraharmonic (4:1) resonance. The associated pattern speed is 86.0 km s^{-1} kpc^{-1}. However, it is less clear which feature is actually setting up this pattern.

The outer ring, which has a size of $\simeq 6.3 \times 5.9$ kpc, contains roughly two-thirds of the total H I mass, and has bluer colours and more intense Hα emission than the main disk. A Fourier analysis of the $B-I$ colour along this ring suggests that it is composed of 9 blobs, indicating the existence of a bead instability. This is in agreement with a simple calculation showing that the number of Jeans lengths along the ring is also 9, and that self-gravity is probably important here.

Clumps also exist in the inner pseudoring, but they are less well defined, and there is no H I concentration along it. This ring has redder colours than the outer ring. The blue inner ring is incomplete, coincides with a complete and intense Hα ring, and is surrounded by a redder ring. A spiral-like structure extends from the inner ring out to the inner pseudoring, with the same winding direction as the outer flocculent arms.

We have constructed a mass model, from which we obtain a mass-to-I-band luminosity ratio of 5.1 for the bulge, and 1.8 for the disk. The core radius of the halo is 11.0 kpc, and its central density 0.062 M$_\odot$ pc^{-3}. The ratio of halo core radius to optical radius is thus of order unity.

Key words: galaxies: spiral; kinematics and dynamics; structure; NGC 7217

Send offprint requests to: L. Verdes-Montenegro

1. Introduction

Rings and pseudorings are observed mainly in barred disk galaxies, and are thought to be associated with orbital resonances produced in non-axisymmetric mass distributions. This idea has first been suggested by Schwarz (1981), who studied the response of a gaseous disk to a rotating stellar bar. Athanassoula et al. (1982) made a statistical analysis of sizes of rings, and find that their positions in barred galaxies are associated with the main dynamical resonances. Further studies have supported this interpretation, either from a theoretical point of view (e.g. Schwarz 1984a, b, c, 1985) or from more detailed observational material (e.g. Buta 1986 and Buta & Crocker 1991). Thus the observational study of rings in barred spirals can provide information on the pattern speed of the non-axisymmetric gravitational potential.

However there are ring systems in which the bars are weak or even non-existent. Since the origin of these rings is not yet understood it is important to study such systems observationally. For this reason we have studied the morphology and kinematics of the H I emission in the highly symmetric ringed galaxy NGC 7217. De Vaucouleurs & Buta (1980) measured the ring diameters from optical images, obtaining $\sim 0'.35$ for an inner ring, $\sim 1'.10$ for an inner pseudoring and $\sim 2'.50$ for an outer ring. The inner ring is particularly clear in Hα images, as shown by Keel (1983) and Pogge (1989).

In this paper, we present 21 cm observations and CCD-$BVRI$ photometry of this galaxy, classified as (R)SA(r)ab by de Vaucouleurs et al. (1991). A detailed description of its optical appearance can be found in the Hubble Atlas (Sandage 1961). Peterson et al. (1978), from an integrated H I profile of the galaxy (beam $\simeq 10'$), note a low hydrogen content for its luminosity and type, as compared to four other Sab galaxies. An integrated profile of the CO(1−0) emission has been obtained by Verter (1987), with a beam size of $\simeq 1'.7$. From Hα spectrophotometry by Kennicut & Kent (1983), Kennicut (1983) derives a star formation rate of 2.7 M$_\odot$ yr^{-1}, a value normal for its morphological type.

The systemic heliocentric radial velocity of this galaxy, obtained from our H I data and corrected to the centroid of the Local Group, is 1239 km s^{-1}, which, for a Hubble constant of

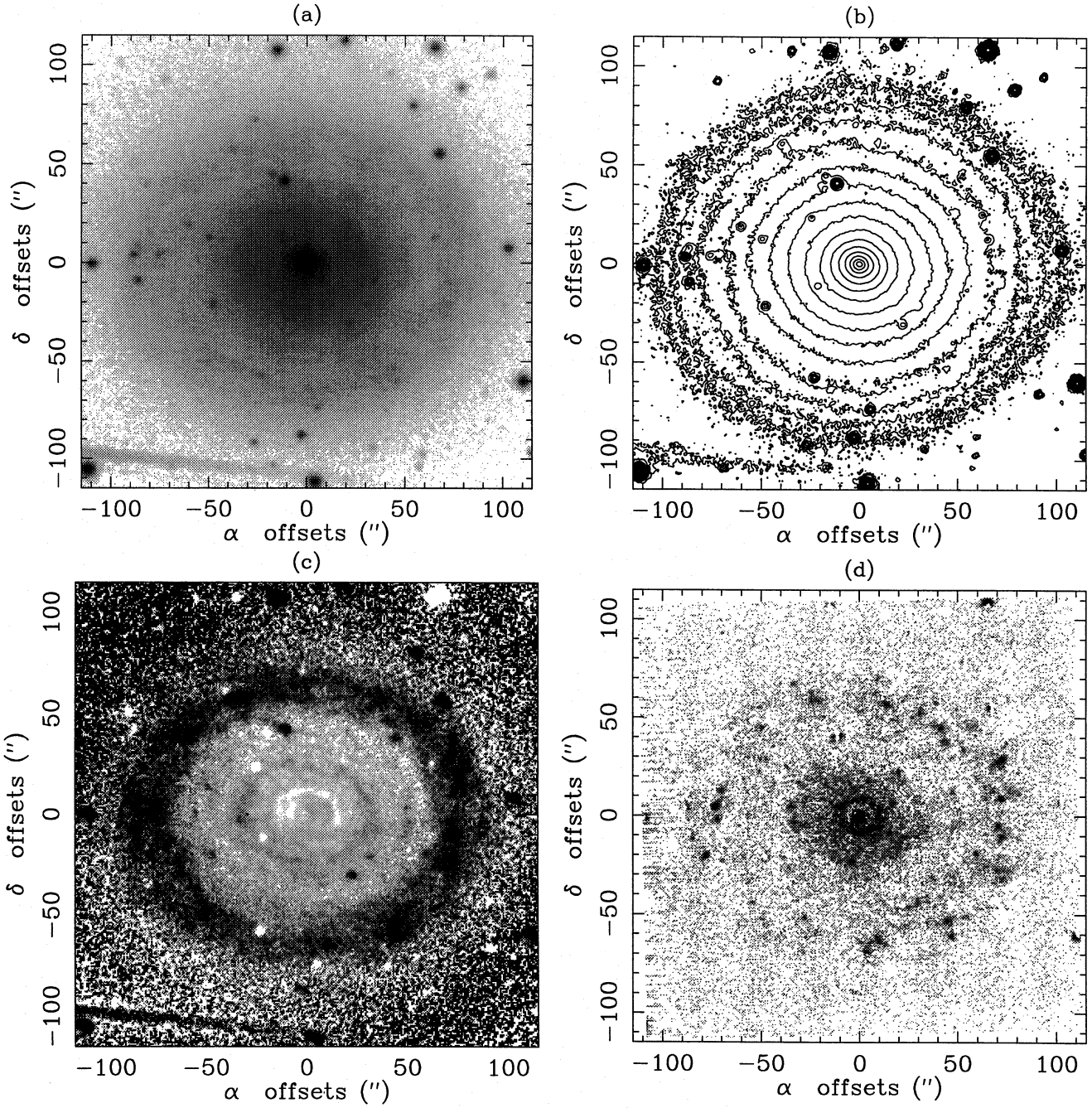

Fig. 1a–d. **a** B image of NGC 7217 in a logarithmic grey scale representation. **b** Isophotal contours corresponding to the I filter image, ranging from 15 to 22 mag/(″)^2, with a step of 0.5. **c** $B-I$ colour image in a grey scale ranging from 1.5 (black) to 2.2 (white) magnitudes. Colours have been corrected for interstellar absorption. **d** Hα image supplied by R. Pogge. Higher intensities are darker. The orientation of all the images is north up and east to the left

75 km s^{-1} Mpc^{-1}, gives a distance of 16.4 Mpc. The galaxy appears to be relatively isolated on the sky. From Tully's Nearby Galaxy Catalogue (Tully 1988), we find that the nearest galaxy is NGC 7292, a magellanic irregular at a projected distance of 4.5 degrees, which at the distance of NGC 7217 corresponds to 1.3 Mpc. The nearest bright galaxy is NGC 7331 at a projected separation of about 2.0 Mpc.

2. Observations and data analysis

2.1. Photometry

We obtained CCD images of this galaxy in the *BVRI* bands at the Newtonian focus of the 1.20 m telescope of the Observatoire de Haute Provence (France) using a Tektronix CCD camera with 512×512 pixels, and a scale of 0.″77/pixel. The exposure times were 40, 20, 16, and 14 minutes in B,V,R and I, respectively,

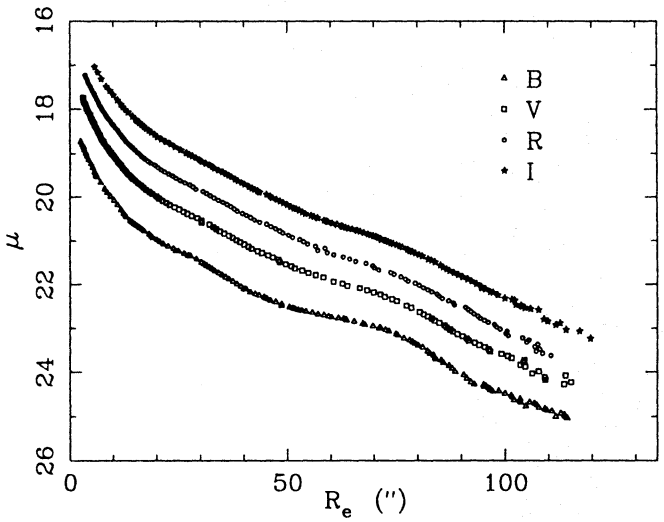

Fig. 2. Averaged radial profiles in each individual photometric pass band as a function of the equivalent radius of each isophotal level

and the seeing was $\sim 2''.2$ FWHM. The reduction and calibration of the data were performed in a standard way. The atmospheric extinction was determined through observations of two selected fields in the open clusters M67 and NGC 7790, and the rms errors in the standard stars in the final calibration are smaller than 0.05 mag in B, 0.02 mag in $B - V$ and $V - R$, and 0.03 for $R - I$.

From these images we obtained the relevant photometric parameters of NGC 7217. First stars, as well as H II regions, were masked. Then we calculated the equivalent radius (defined as the radius of a circle having the same area delimited by the isophote) for each isophotal level of the four observed photometric bands, getting in this way the azimuthally averaged radial luminosity profile as a function of galactocentric radius. Finally we fitted ellipses to the isophotes, inferring in this way their ellipticities and position angles.

2.2. Radio observations

Observations of the 21 cm line of H I were made with the Westerbork Synthesis Radio Telescope (WSRT[1]) during 1983. We used 40 interferometers with spacings ranging from 36 m to 2700 m in steps of 72 m. This results in a synthesized beam of $13''.0 \times 24''.9$ ($\alpha \times \delta$) and first grating response at $10' \times 17'$ ($\alpha \times \delta$). We used a digital backend (Bos et al. 1981) resulting in 32 channel maps at heliocentric velocities 707.6 to 1202.3 km s^{-1}. Hanning smoothing was applied on-line, giving a velocity resolution of 33.0 km s^{-1}.

The data were edited and calibrated using the standard WSRT tasks for calibration and Fourier transformation (Högbom & Brouw 1974). At this stage of the data processing

[1] The Westerbork Synthesis Radio Telescope is operated by the Netherlands Foundation for Radio Astronomy with financial support from the Netherlands Foundation for the Advancement of Pure Research (Z. W. O.)

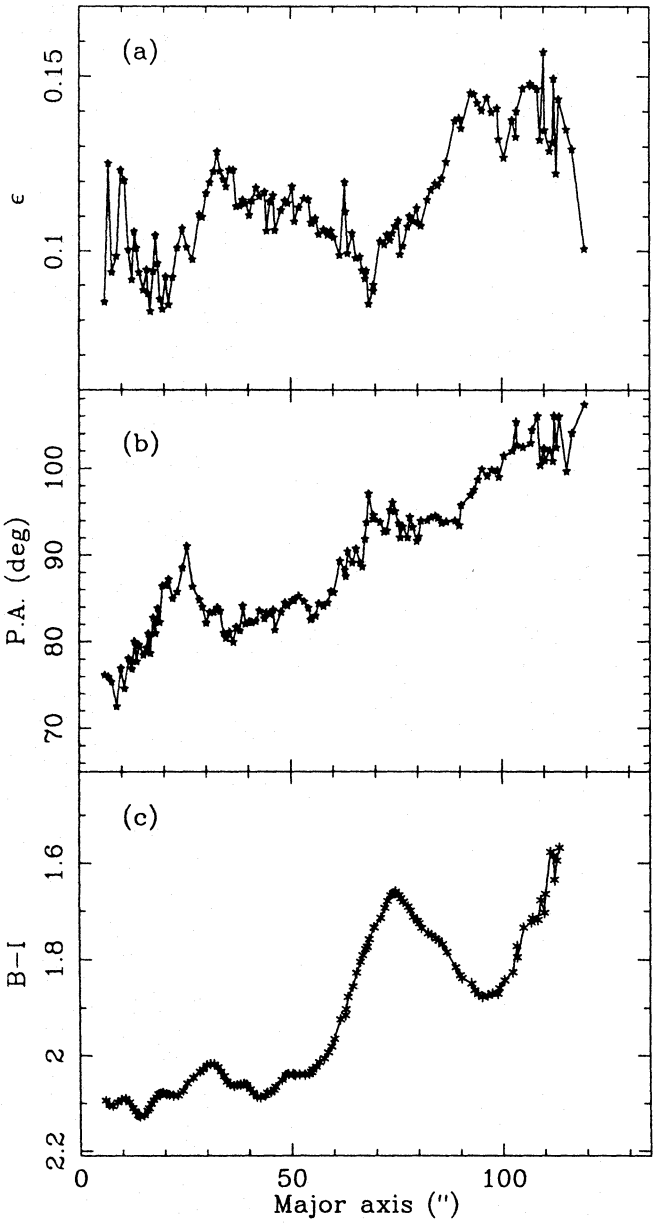

Fig. 3a–c. **a** Ellipticity, **b** position angle and **c** radial colour index profile ($B - I$) of the ellipses fitted to the isophotes as a function of their semi major axis length (see Sect. 3.1). Angles are measured from north to east

the line radiation of the galaxy in each map is still superposed on the continuum radiation from both the galaxy and background sources. The average of the line-free channels 1 to 4 and 27 to 29 has been subtracted from all the individual channels. A rms noise level of ~ 0.8 mJy/beam was achieved after 12 hours of integration. To get better sensitivity in the central parts of the galaxy, we convolved the map data with a gaussian, leading to a beam size of $18''.4 \times 35''.2$ ($\alpha \times \delta$). We used these maps to construct the integrated H I distribution and associated radial velocity field (see Sect. 3.3). Primary beam corrections away from

the phase centre have not been applied to our maps, since the emission is concentrated within the 98% of its peak response.

3. Results

3.1. Optical emission

We present in Fig. 1a the calibrated B band image of NGC 7217 using a logarithmic grey scale representation. The flocculent pattern of its spiral structure can be noted. In Fig. 1b we show the isophotal map corresponding to the I image which shows the high symmetry of this galaxy. The rings are clearly evident in both Fig. 1c and 1d, where we present respectively our $B-I$ colour image and a Hα image kindly provided by Dr. Richard Pogge. Colours have been corrected for galactic foreground absorption using the extinction value given by Burstein & Heiles (1984), with the reddening law from Savage & Mathis (1979).

We have obtained, as described in Sect. 2.1., the averaged radial brightness profiles, together with the ellipticities and position angles of the ellipses fitted to the isophotes, in the four observed bands. In Fig. 2 we plot the radial brightness profiles as a function of the equivalent radius of the corresponding isophotal level. Two noticeable humps are present, which are increasingly pronounced as we go from the I to the B filter. They correspond to the outer ring and inner pseudoring measured by de Vaucouleurs & Buta (1980), located at equivalent radii $\simeq$ 70″ and 30″ respectively.

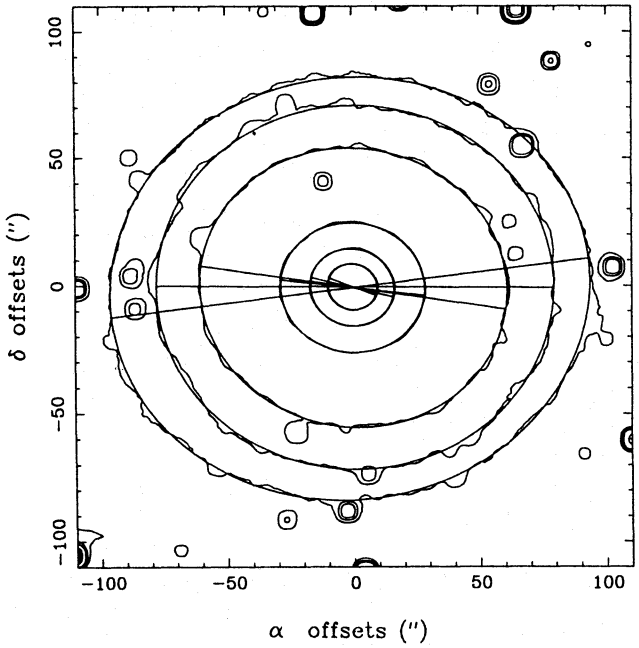

Fig. 4. Isophotes for the I image (smoothed with a boxcar of 3×3) at the positions of the local extrema of ellipticities and position angles (see Fig. 3). We have superposed the fitted ellipses, together with their major axes

Table 1. Parameters of NGC 7217

Centre position[a]	
α(1950.0)	$22^h\ 05^m\ 37\overset{s}{.}89$
δ(1950.0)	31° 06′ 51″.25
Inclination[a]	28°
Position angle[a]	89°
B_T^0 [b]	10.52
Systemic heliocentric velocity	
Optical[c,d]	947.5 km s^{-1}
H I[a]	947 km s^{-1}
Distance[a]	16.4 Mpc

[a] This paper. [b] de Vaucouleurs et al. 1991. [c] Peterson et al. 1978. [d] Rubin, Ford & Thonnard 1982

The results for the fitted ellipses are shown in Fig. 3a and b, where we give respectively the ellipticity of the ellipses fitted to the isophotes and their position angle, as a function of their major axis. We can see a tendency for the ellipticity to increase from the center to a value of 0.12 for the outer isophotes, with local variations between the rings. The position angles of the ellipses present a clear increase with semi-major axis length, with some local extrema roughly coinciding with those of the ellipticity. The isophotes corresponding to these extrema can be visualized in Fig. 4 together with the corresponding fitted ellipses and their major axes. The variations in position angles are in the direction of rotation of the galaxy (assuming spiral arms are trailing). We have to note that for ellipticities smaller than 0.07 the position angle determinations are not reliable. No significative variations have been found for center positions of the isophotes. Further analysis of the ellipticities of the isophotes requires deprojection. Assuming a pure disk component for the outer isophotes, we obtain an inclination of the galaxy of 28° to the line of sight. Deprojection of this galaxy will be further discussed in Sect. 4.

The radial colour index profile has been calculated from the two-dimensional colour distribution shown in Fig. 1c. This image has been integrated in elliptic annuli of 3″ width and with the geometrical parameters corresponding to the I isophotes. We choose this colour since its smoother light distribution allows a more accurate fitting to the isophotes. The corresponding colour profile is shown in Fig. 3c. In Table 2 we present the geometrical parameters of the rings, together with their characteristic colours corrected for galactic foreground absorption.

3.2. 21-cm continuum emission

The channel maps free of line emission were averaged into a map of the continuum radiation. We cleaned this map and found a central source with an integrated flux density of 7.4 mJy ± 0.6 mJy. Its position (α(1950) = $22^h\ 05^m\ 37\overset{s}{.}78$, δ(1950) = 31° 06′ 51″.2) is coincident, within the beam, with that of the optical centre (cf. Table 1). The source was nearly resolved, having a Gaussian size of $\sim 26'' \times 15''$, which means a deconvolved

Table 2. Rings parameters

Ring	Semimajor axis (arcsec)	Semiminor axis (arcsec)	Position angle (°)	$B-I$	$B-R$	$B-V$
Outer	79.1	73.8	104.5	1.5-1.7	0.8–1.2	0.5–0.7
Inner pseudo	32.0	28.4	78.5	1.8–2.0	1.4	0.8
Inner red	14.4	12.7	74.6	2.2	1.6	0.9
Inner blue	10.9	9.7	90.5	2.0	1.4	0.8

Table 3. Derived parameters

H I flux[a]	11.7 Jy km s^{-1}
H I flux[b]	14.3 Jy km s^{-1}
$M_{\rm HI}$	7.4 × 10^8 M$_\odot$
$M_{\rm HI}/L_B^0$ [a]	0.03
$M_{\rm bulge}$ (out to 9.7 kpc) [a]	5.8 × 10^{10} $M_\odot$
$M_{\rm disk}$ (out to 9.7 kpc) [a]	2.8 × 10^{10} $M_\odot$
$M_{\rm halo}$ (out to 9.7 kpc) [a]	15.8 × 10^{10} $M_\odot$

[a] This paper. [b] Peterson et al. 1978

Table 4. Rotation curve

Radius (arcsec)	(kpc)	Rotation velocity (km s^{-1})	rms error (km s^{-1})
2.17	0.17	128.0	34.9
7.96	0.63	249.5	22.5
12.05	0.96	284.3	9.8
17.09	1.36	298.5	10.8
22.02	1.75	323.4	11.7
26.91	2.14	317.8	15.7
31.89	2.54	319.0	16.7
35.88	2.85	306.4	24.4
47.77	3.80	303.3	12.0
52.99	4.21	313.3	5.3
65.40	5.20	303.0	4.0
75.00	5.96	301.8	3.7
85.00	6.76	303.4	3.0
95.00	7.55	312.0	3.9
105.00	8.35	320.1	6.1
115.00	9.14	332.4	9.6
125.00	9.94	340.7	8.0

size of $\sim 10'' \times 8''$, similar to the inner ring. However this coincidence has to be taken very carefully, since deconvolution with source sizes close to the beam size leads to a high imprecision in deconvolved sizes. We detected a second double source at $\alpha(1950) = 22^{\rm h}\ 05^{\rm m}\ 28\overset{\rm s}{.}99$, $\delta(1950) = 31°\ 09'\ 14\overset{''}{.}1$ and $\alpha(1950) = 22^{\rm h}\ 05^{\rm m}\ 25\overset{\rm s}{.}16$, $\delta(1950) = 31°\ 08'\ 46\overset{''}{.}0$, with an integrated flux of 2.0 mJy ± 0.6 mJy.

3.3. The ringed H I distribution

In Fig. 5 we display the full resolution channel maps containing the H I emission at the observed radial velocities, with a channel width of 16.5 km s^{-1}. These channel maps show the usual pattern of differential rotation. The approaching and receding parts of the galaxy are quite symmetric, within the resolution of our observations.

For an overall view of the H I structure we determined the integrated H I column density distribution as follows. The channel maps were smoothed with a gaussian tapering function (see Sect. 2.2) and manually "blotted" to exclude regions of sky where no emission was detectable. Then we added up those pixels in the channel maps where the emission intensity exceeds the rms noise (1σ) in these blotted and smoothed channel maps. Superposed on our optical $B-I$ colour image of NGC 7217 we show in Fig. 6 a contour representation of the total H I column density distribution.

The extent of the atomic gas is similar to that of the optical emission. Furthermore, the higher column densities occur at the region of the optical outer ring. A relative H I depression exists in the part of the galaxy within the outer ring, with three minima in the gas distribution. We have detected no excess H I emission corresponding to the optical inner pseudoring. Towards the centre a slight enhancement of the H I column density exists, which could be associated to the innermost optical ring, but the size of the area is comparable to the beamsize, so no definitive conclusions can be obtained given the resolution of our data.

The total H I gas content of the disk component is 7.4 10^8 M$_\odot$, as estimated from the global profile. This profile, shown in Fig. 7, was obtained by integrating the flux density in each channel map over an area containing the line emission. This mass is compared to that obtained by other authors reduced to our distance scale in Table 3. The good agreement between the H I masses deduced from the single dish and interferometric observations indicates that little atomic gas is located outside the outer ring, and that we did not miss any extended H I emission in our maps.

The H I profile shows a typical two horned shape together with an extra peak at ~ 920 km s^{-1}. This feature is associated to the clump that we have detected in the H I column density toward $\alpha(1950) = 22^{\rm h}\ 05^{\rm m}\ 50\overset{\rm s}{.}75$ $\delta(1950) = 31°\ 06'\ 18\overset{''}{.}5$, at a projected distance of $2\overset{'}{.}8$ of NGC 7217. No optical emission appears to be associated to it.

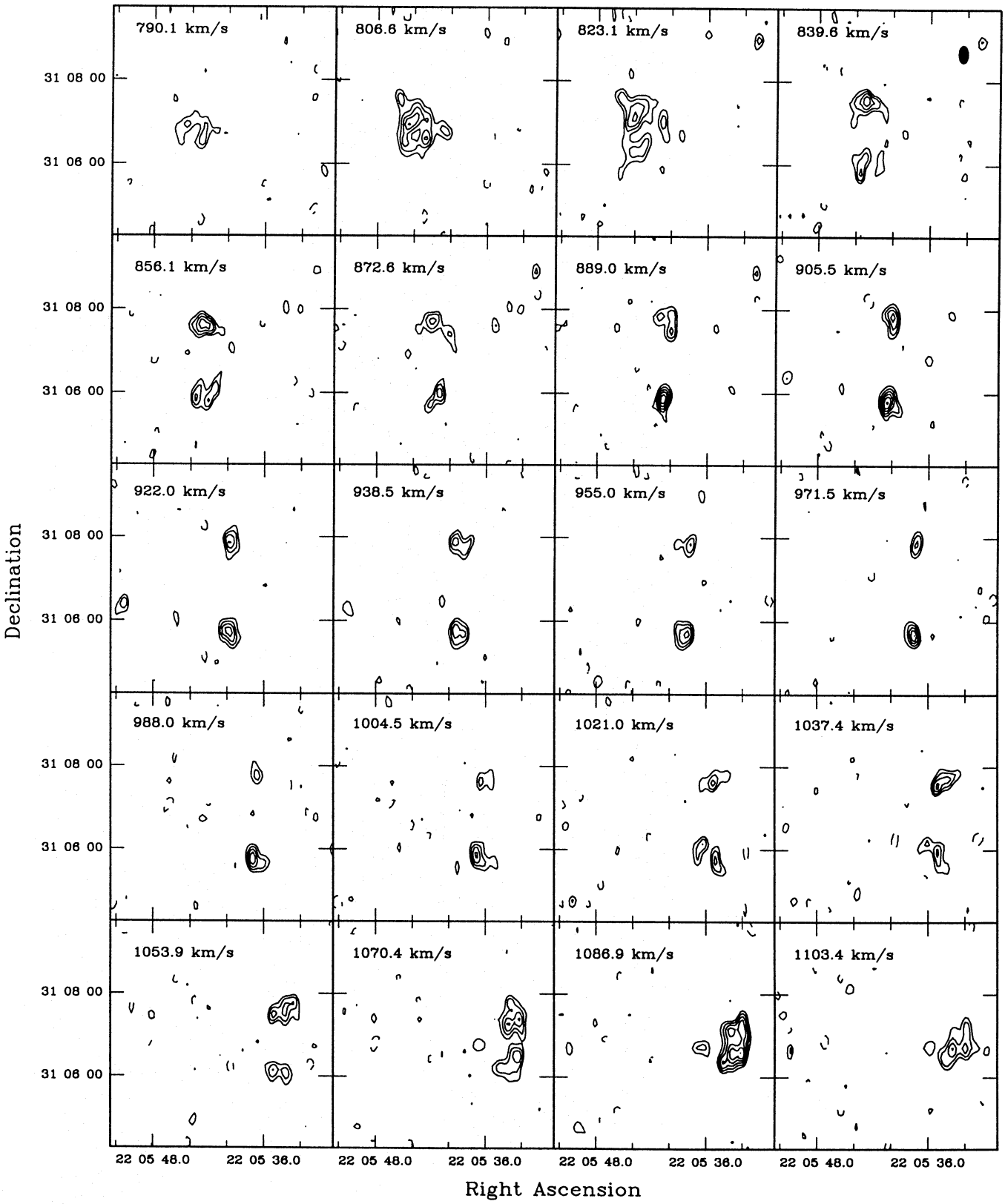

Fig. 5. Channel maps of the 21 cm line radiation. The heliocentric velocities are as indicated in each panel. Contours correspond to −3.7, 3.7, 5.2, 6.7, 8.14, 9.6, 11.1 and 12.6 K, and the rms noise of the maps is 1.48 K. Synthesized beam = 13.″0 × 24.″9 ($\alpha \times \delta$)

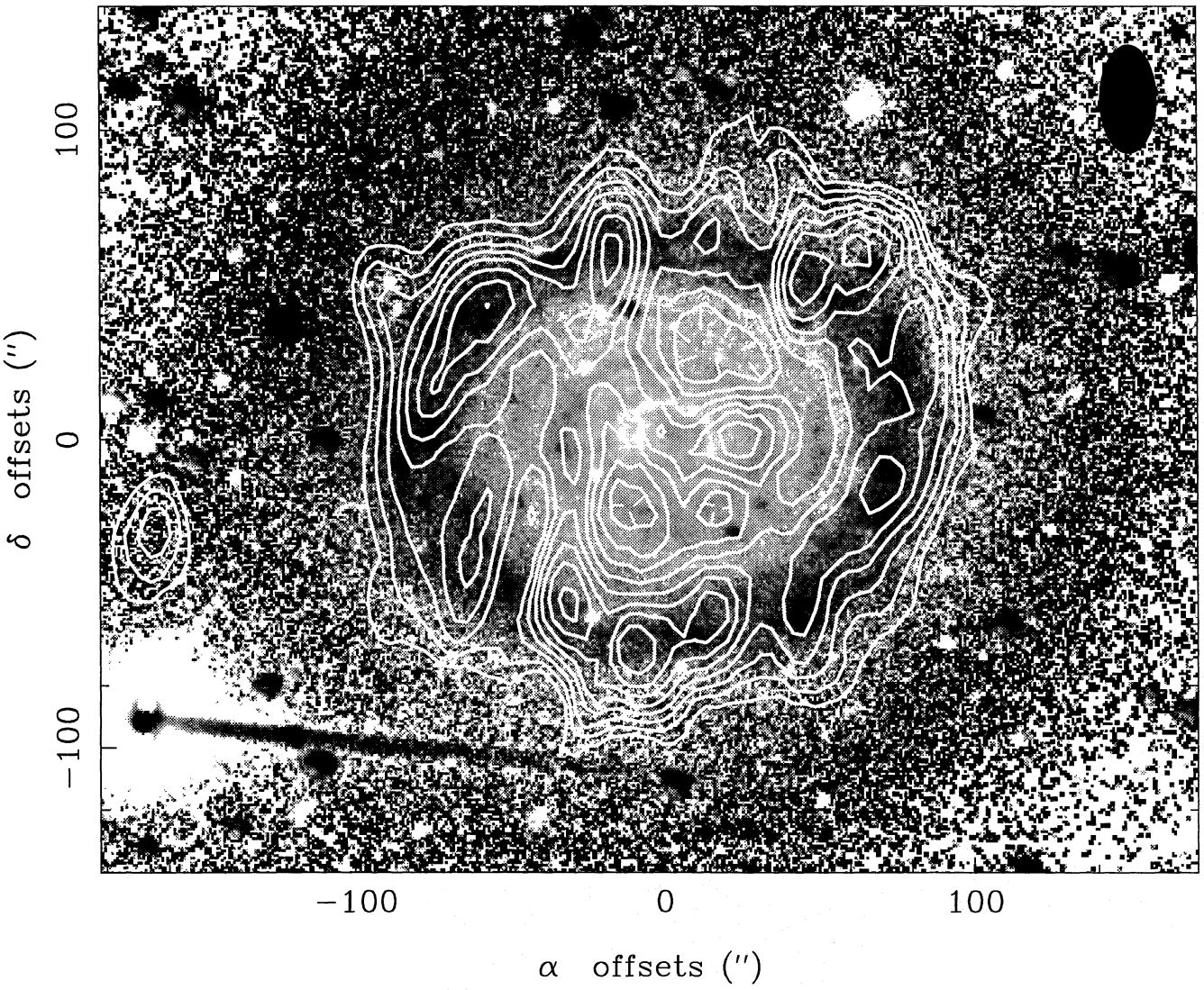

Fig. 6. Map of the H I column density distribution in NGC 7217, superimposed on the $B - I$ colour image. The contour interval is 0.9 10^{20} atoms cm^{-2}, and the first contour corresponds to 1.8 10^{20} atoms cm^{-2}. Synthesized beam = 18.″2 × 35.″4 ($\alpha \times \delta$). $B - I$ image is as in Fig. 1c

3.4. H I velocity field

In order to study the kinematics in a systematic way, we derived the intensity weighted mean radial velocity field, in a similar manner as the total integrated emission (see Sect. 3.3). Because of the low inclination, the profiles at each position in the sky are nearly symmetric and the first moment of the data cube is a good approximation for the radial velocity of the bulk of the H I. The result is shown in Fig. 8.

It can be seen that there is little deviation from the characteristic shape of a disk in circular differential rotation. The bumps of the isovelocity contours toward the centre are coincident with local enhancements of the H I emission with a size scale of the order of the beam. At the individual spectra these bumps show up as asymmetries in the profiles with an intensity smaller than 3σ. Therefore we do not consider them to be significant.

4. Discussion

4.1. Spatial orientation of the galaxy

In this section we discuss the choice of the position and inclination angles, necessary for deprojecting the galaxy. We have explored four possibilities which can be considered as independent, since two are based on our photometrical data, one on our H I data, and one on the spectroscopical results for the optical rotation curve: a) If the outer isophotes are circular, the inclination of the galaxy would be $i = 28° \pm 1°$ and its position angle p.a. = 100° ± 1°. Using this values to deproject the I image we obtained the profiles of ellipticity and position angle of the isophotes in the same way as in Sect. 3.1. These are shown in Fig. 9a, where we have also indicated the positions of the rings from the $B-I$ colour image, deprojected in the same way. It can be seen that ellipticity decreases with radius, with small peaks

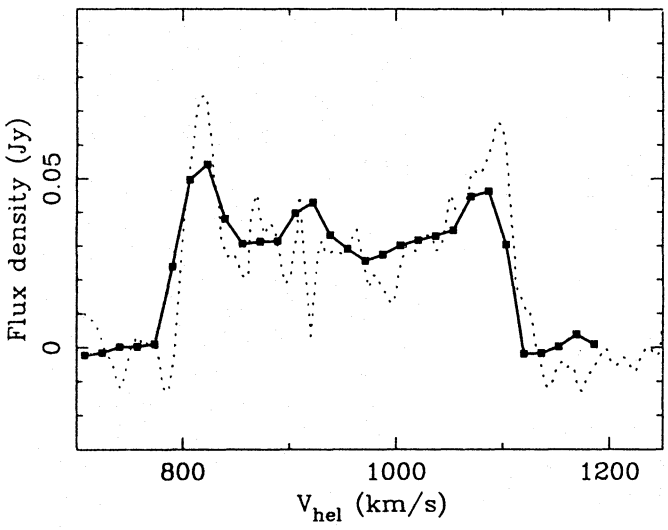

Fig. 7. Comparison of the integral H I profiles of the galaxy: thick line from this paper, dotted line from Peterson et al. (1978)

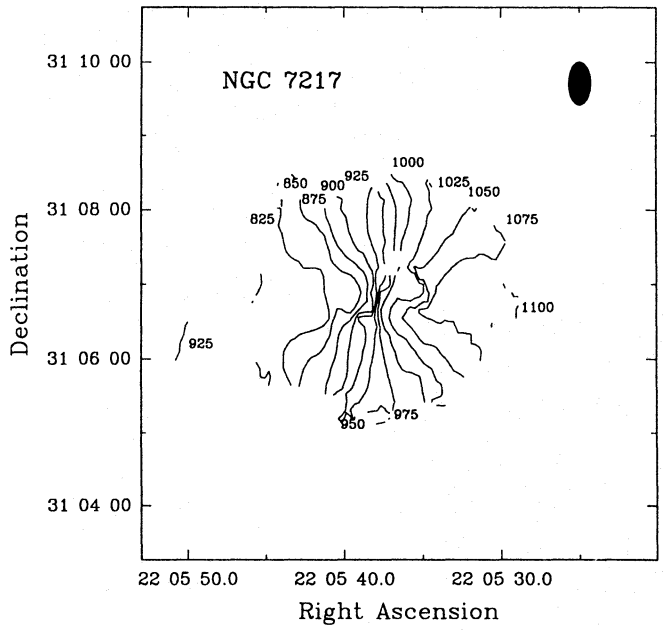

Fig. 8. Map of the first-order moment of the radial velocity field in NGC 7217. The numbers indicate heliocentric velocities in km s^{-1}. Synthesized beam = 18.″2 × 35.″4 ($\alpha \times \delta$)

overlapped to this tendency. The large fluctuations of the position angle obtained for the lower ellipticities are meaningless, since an accurate determination is not possible for such cases. b) The second possibility is to consider that, although rings can be intrinsically oval, the region between the inner pseudoring and the outer ring would have circular isophotes. If this condition is fulfilled, we obtain the same inclination as for the previous case, i.e. $i = 28° \pm 1°$, and a value for the p.a. of 85° ± 1°. The isophotal parameters obtained with this deprojection are shown in Fig. 9b. c) A reanalysis of the optical radial velocities also indicates an inclination of 28° ± 3°, and a position angle of 82° ± 2°. The parameters of the isophotes for the deprojected I image are shown in Fig. 9c. It is interesting to note that all three so-far considered solutions give the same value of 28° for the inclination of NGC 7217. d) The most reliable estimate for the position angle is usually obtained from the H I velocity field. When determining the rotation curve for the H I emission, as explained in Sect. 4.2, we found the lower errors for a position angle of 89° ± 1°, and inclinations in the range of ∼ 24–32°. Since this method is relatively insensitive to the inclination angle, we will choose from the range it outlines the value of i = 28°, based on the results of the other three explored possibilities. The ellipticity and position angle profiles are shown in Fig. 9d. By comparing the four cases we can say that for position angles, a value of 89° is the one that gives more reasonable results, both for the H I velocity field, and for the behaviour of the so deprojected I Image (Fig. 9d). In this figure we can notice that low ellipticities are achieved along all the radii, with several small amplitude local peaks. The change in position angle by 90° at 65″ radius indicates that the minor axis becomes suddenly major axis due to the very low value of the ellipticities : it can be concluded that this hints to the existence of a very mild oval distortion in which case the outer ring is perpendicular to the inner oval. Thus, for all further work we will adopt a p.a. of 89° and an inclination of 28°, since these values are the best for the H I velocity field and are quite reasonable for the photometric data.

4.2. Rotation curve and mass model

In order to determine the rotation curve we assumed circular rotation and modelled the velocity field with a least-square algorithm based on a tilted ring model as described in Begeman (1987, the ROTCUR task in Gipsy). By this procedure we divided the galaxy into concentric rings, each of them with a width of 10″ along the major axis. The symmetry of the H I distribution lead us to average the approaching and the receding part of the galaxy when determining the rotation curve parameters. Points within a sector of ± 30° from the minor axis were excluded from the fits. The centre position was fixed to the position of the optical center as obtained from our photometry, with an accuracy of 0.″5. A first estimate of the systemic velocity has been obtained from the integrated H I emission, as the central velocity for a half maximum intensity, namely 950 km s^{-1}. Then a very stable value of 89° was found for the position angle and inclinations in the range of $\sim 24 - 32°$. Since this method is relatively insensitive to the inclination angle, we have taken from the range it outlines the value of $i = 28°$, which agrees with the results obtained with the 3 first methods exposed in Sect. 4.1. A final iteration gave a final result for the systemic velocity of 947 ± 1 km s^{-1}.

We also constructed a rotation curve based on optical data alone, derived from the radial velocities listed by Peterson et al. (1978), and those derived from spectra kindly made available to us by M. Moles and I. Márquez and analyzed by us. This curve is higher than the observed H I curve at radii smaller than ∼ 50″. It can be argued that the differences are produced by

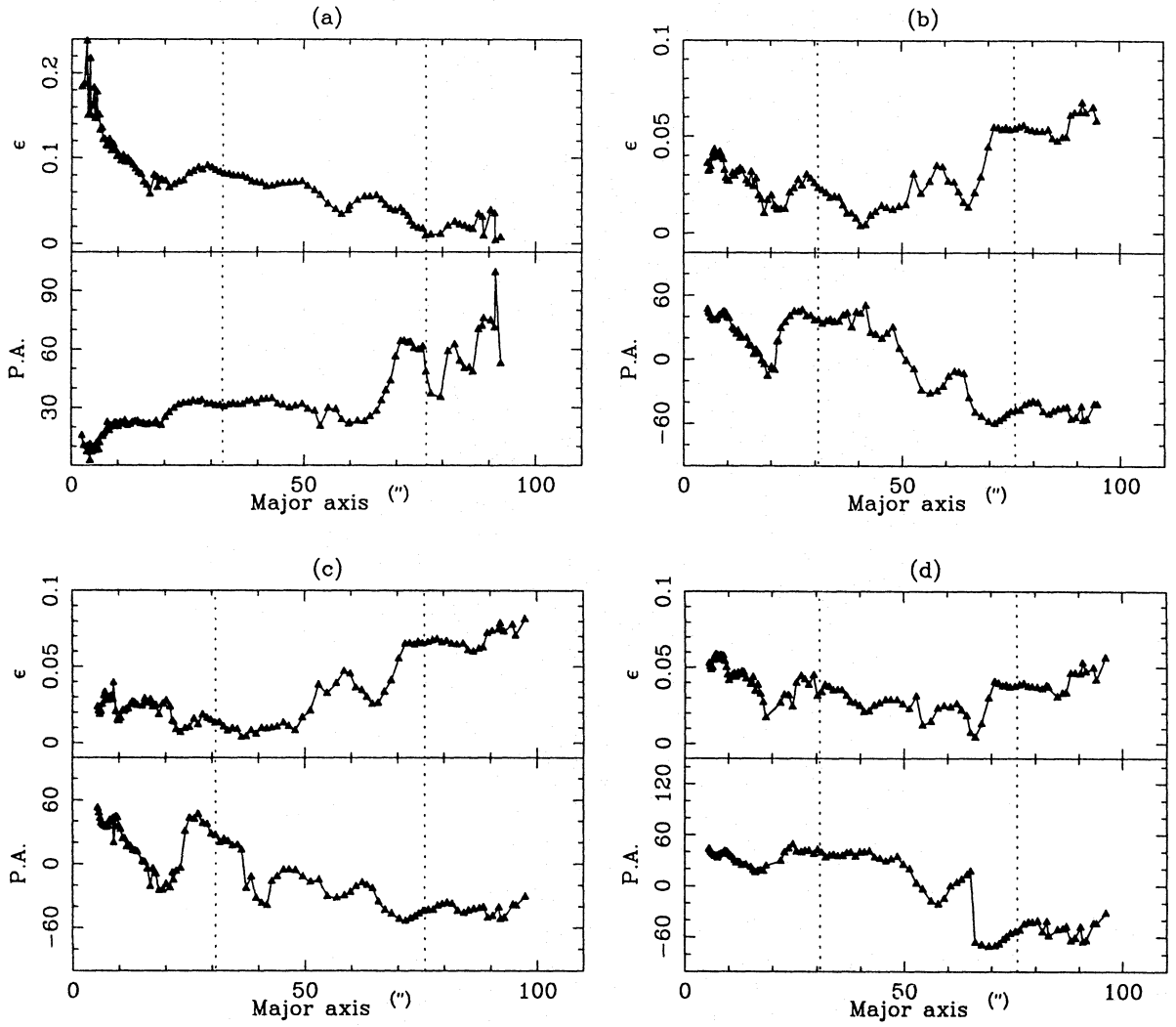

Fig. 9a–d. The upper panels show the ellipticity of the ellipses fitted to the isophotes as a function of their major axis and the lower panels their position angle for I image obtained after deprojection, with the following parameters: **a** p.a. = 100°, i = 28° **b** p.a. = 85°, i = 28° **c** p.a. = 82°, i = 28° **d** p.a. = 89°, i = 28°, in correspondence with the 4 cases analysed in the text, Sect. 4.1. We have also marked, with dotted lines, the positions of the outer ring and inner pseudoring, as obtained from the radial colour index profile corresponding to the deprojection of the $B-I$ image with the same parameters. Distances are measured along the major axes of the ellipses fitted to the isophotes

beamsmoothing: since the beam is elongated along the minor axis the integration effect is such that the radial velocities are always biased towards values lower than the true values corresponding to the rotation curve. We thus combined the optical and radio data into one curve, by adopting the optical data out to 55″ and the H I data for the outer six points. Points in between have been added to assure a smooth continuation. The result is summarized in Table 4, where the errors reflect the errors in the mean. The slight rise in the very outer parts may not be very significant due to the uncertainties in the deprojection.

We have constructed a mass model for NGC 7217 based on our photometric data and the combined optical/H I rotation curve (see Athanassoula et al. 1987 for an extensive description of the mass model procedures). From our I photometric radial luminosity profile, assuming constant mass-to-light ratios for bulge and disk separately, we calculate the expected rotation curve for the luminous mass in the galaxy. For the outer ring however we use simply an interpolation, so as not to give undue weight to the blue star forming regions, in which the mass to luminosity ratio is likely to be lower. We have thus calculated a maximum disc solution with no hollow core, which we show in Fig. 10. For the gas, we correct for helium with a factor 1.36, but we do not correct for molecular hydrogen, which is assumed to follow the light distribution. The resulting mass-to-I-luminosities not corrected for absorption are 5.1 for the bulge, and 1.8 for the disk, which fall within the range found by Athanassoula et al. (1987) for a galaxy of morphological type Sab. The core radius of the halo is 11.0 kpc, its central density 0.062 $M_\odot$ pc^{-3} and its velocity dispersion 212.1 km s^{-1}. The ratio of halo core radius to optical radius is thus of order unity.

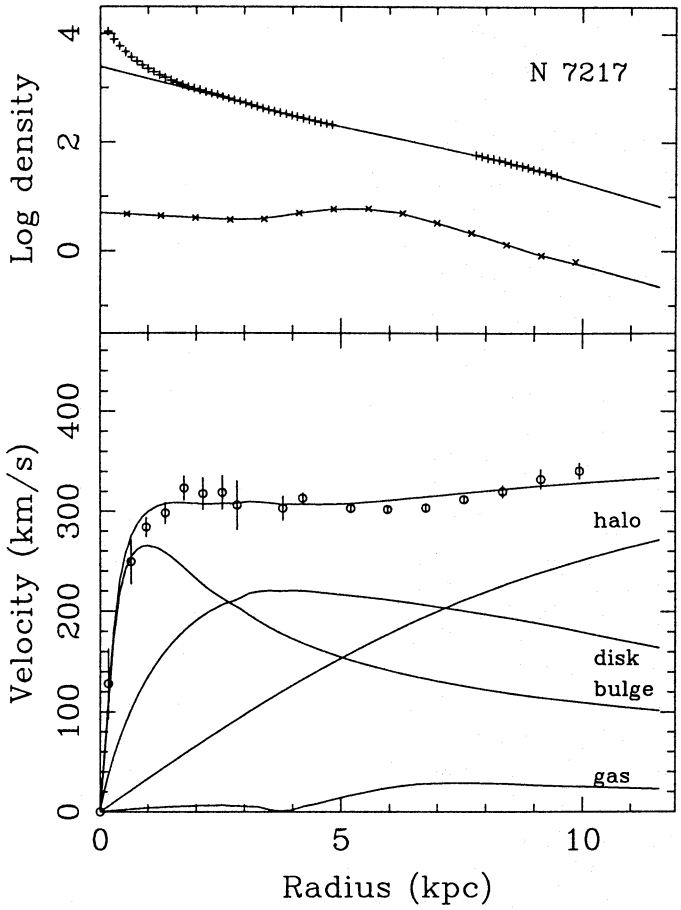

Fig. 10. Composite bulge/disk/gas/halo mass model for NGC 7217. In the top panel the radial distributions of the stellar (plusses) and gas (crosses) components are given in units of $M_\odot$ pc^{-2}. The gap of crosses corresponds to the outer ring cross section, which has been substituted by an interpolation (See Sect. 4.2.). In the bottom panel the rotation curves are shown for each of the components (labelled curves), the best fitting total curve, and the observed rotation curve (circles with error bars, cf. Table 4)

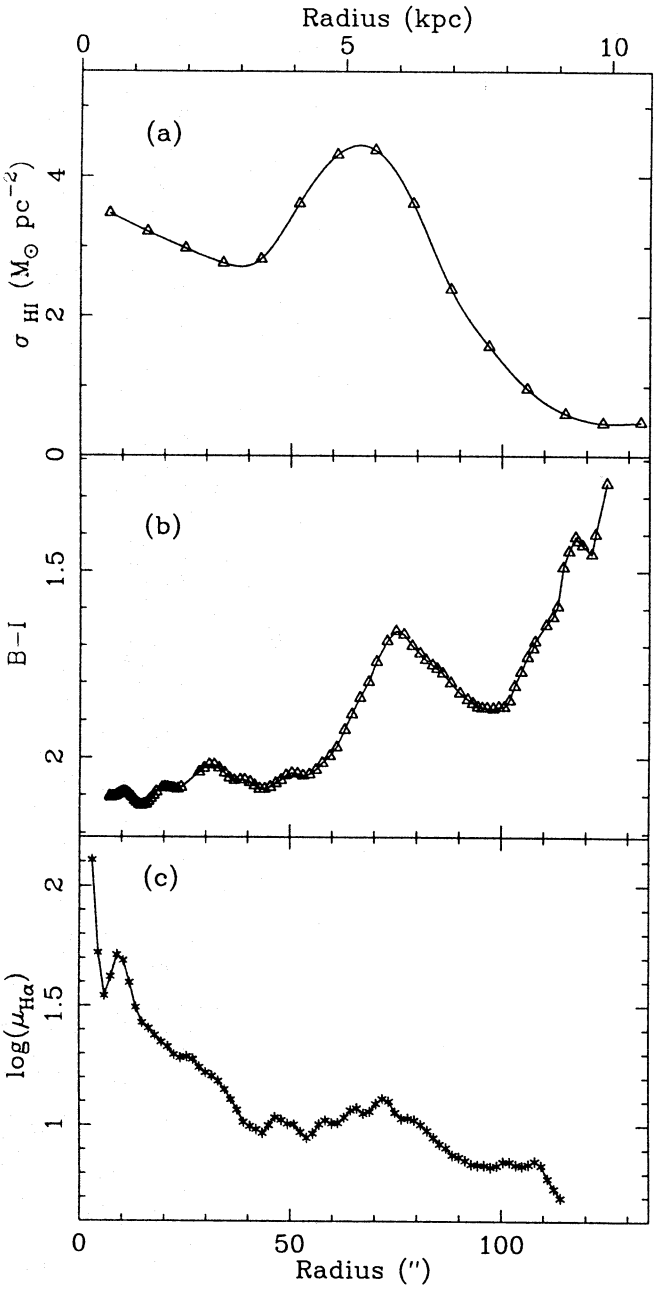

Fig. 11a–c. Radial profiles obtained by integrating in annuli of 3″ thickness of the H I surface density (**a**) $B-I$ colour image (**b**) and Hα image (**c**), deprojected with a p.a. of 89° and i = 28°. The lower radial scale is in arcsec and the upper one in kpc, for a distance of 16.4 Mpc. The scale of the Hα image is logarithmic and not calibrated

4.3. Mass, luminosity, and derived parameters

Out to the optical radius of 9.7 kpc, we find from our mass model that the mass of the bulge, disk and halo component are 0.28 10^{11} $M_\odot$, 0.58 10^{11} $M_\odot$, and 1.58 10^{11} $M_\odot$, respectively. From CO(J=1-0) observations, Verter (1987) derives an H_2 mass of 10^9 $M_\odot$, giving a H_2/H I mass ratio for NGC 7217 of 1.4. The total blue magnitude is B_T^0 = 10.52 (de Vaucouleurs et al. 1991). For a distance of 16.4 Mpc, the blue luminosity is then 2.6 10^{10} $L_\odot$, implying a $M(H_2+HI)/L_B$ = 0.07$M_\odot$ $L_\odot^{-1}$. This ratio is low for an Sab galaxy (cf. Young & Knezeck 1989) implying a high star formation efficiency in the past. Using this blue luminosity, the mass of the galaxy in the form of stars, and the Lyman continuum photon flux, we have explored the star formation history of the galaxy (Gallagher, Hunter & Tutukov, 1984). The star formation rates, obtained as defined in that paper are α_C = 0.47, α_L = 0.75 and α_M = 0.96 (if we count just the stars in the bulge and disk), or α_M = 2.70 (if we adopt the definition of stellar mass in Gallagher et al. and thus include the dark halo inside R_{opt}), which locates NGC 7217 in the group of galaxies with decreasing star formation rate. This results applies to the galaxy globally, while a local enhancement of the star formation is taking place now in the three rings, since they are emitting in Hα (Fig. 1d).

Figure 11a shows the radial distribution of the H I column density, obtained by averaging the density distribution az-

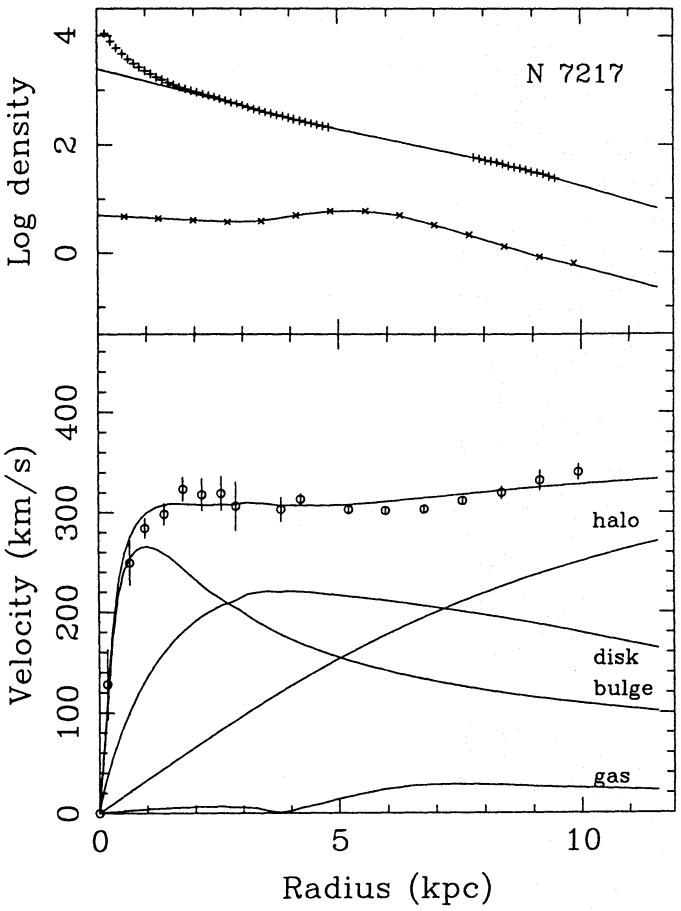

Fig. 12. Angular velocities as functions of radius derived from the fitted curve in Fig. 10: shown are $\Omega - \kappa/2$ (lower full drawn curve), $\Omega - \kappa/4$ (dotted curve), Ω (dashed curve) and $\Omega + \kappa/2$ (upper full drawn curve). The straight line corresponds to a pattern speed of 86.0 km s^{-1} kpc^{-1}

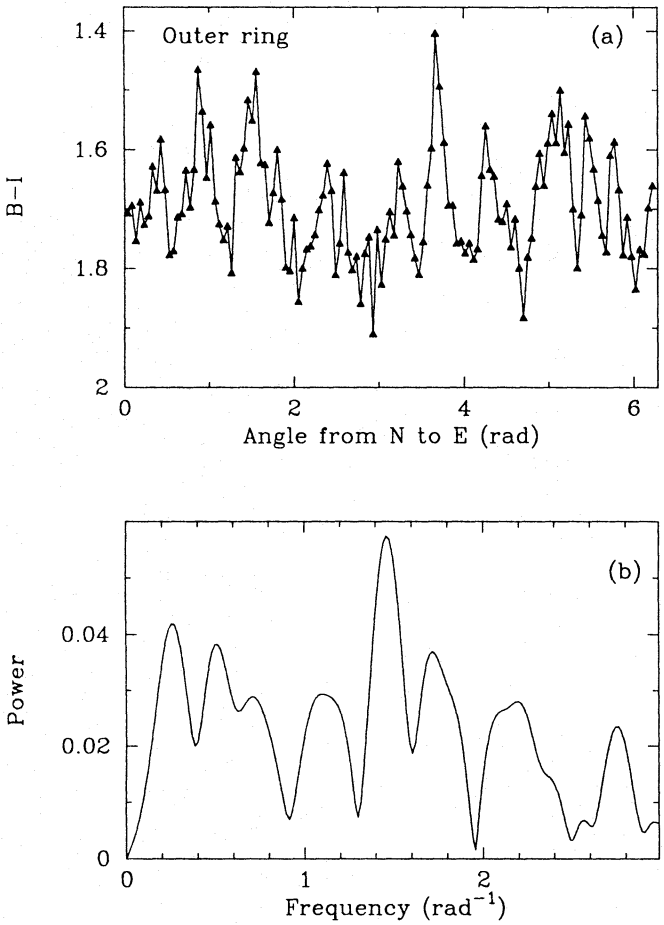

Fig. 13a and b. **a** $B - I$ colour measured as a function of the azimuthal angle along an elliptical annulus located on the outer ring and with a thickness of 10″. Angles are measured from north to east. Colours have been corrected for interstellar absorption. **b** Fourier transform of the colour distribution plotted in **a**

imuthally and corrected for inclination. By measuring the H I mass we find that the sixty six percent is contained in the outer ring comprised between 3.2 and 6.8 kpc.

It may be asked where this galaxy finds itself on the Tully-Fisher relation. If we accept the calibration by Pierce & Tully (1992), and their prescriptions for absorption corrections, we find M_B(expected) − M_B(observed) = −1.26 if we adopt W_R = 635 km s^{-1}. Conversely, if we adopt the M_B (observed) for an Hubble constant of 75 km s^{-1} Mpc^{-1}, we find W_R = 420 km s^{-1}. We would have to change the inclination to 44° to make this galaxy obey exactly the relation given by Pierce & Tully (1992). Hence the galaxy is underluminous for its linewidth, which is principally due to its short extent in radius.

4.4. Ring analysis

(a) The position of the rings and their relation to resonances

The three ring structures could point to the loci of resonances, and it is tempting to identify the outer ring as the outer Lindblad resonance (OLR). If we accept this, we can derive the expected locations of the other resonances from the rotation curve. The observed curve, however, is too poorly determined for this in the inner parts. We thus use the fitted model curve of Fig. 10 to compute the curves of $\Omega + \kappa/2$, Ω, $\Omega - \kappa/4$ and $\Omega - \kappa/2$ as a function of radius, where Ω is the circular angular velocity and κ is the epicyclic frequency. These are given in Fig. 12. The implied positions for the resonances are then 6.3 kpc for the OLR, 3.6 kpc for the corotation radius, 2.3 kpc for the ultraharmonic resonance (UHR, or 4:1 resonance), and 0.6 kpc for the ILR. Obviously, the position of the ILR is a bit uncertain due to the approxiamte nature of the fitted rotation curve there. Thus a pattern speed of 86.0 km s^{-1} kpc^{-1} places all 3 rings at the positions of resonances, the inner one at the ILR, the inner pseudoring at the UHR and the outer one at the OLR.

It is not clear, however, what feature is actually setting up the resonance pattern speed. In such cases the two most obvious candidates area usually a nearby companion, or any m=2 perturbation of sufficient amplitude in the disk, like a bar, oval or massive spiral. We have seen, however, that NGC 7217 is

isolated, while our ellipse fitting did not reveal the existence of any significant oval undetected by visual inspection.

(b) The outer ring

The outer ring is composed of a uniform blue component on which are superposed a set of bluer blobs (Fig. 1c). Probably the focusing of orbits in this ring enhances star formation there and thus its blue colour. For a better understanding of this structure we have studied the $B-I$ intensity measured as a function of the azimuthal angle along an elliptical annulus located on the ring and having a thickness of $10''$ (Fig. 13a). The ellipse is sampled from north to east. Looking at the intensity plot thus obtained, we can see that some type of periodicity exists. To study that, we fourier analysed these data (Fig. 13b). The power spectrum shows a clear peak at $1.46\,\mathrm{rad}^{-1}$. The space scale associated to that frequency is 39°, i.e. we can thus have 9 regular features along the ring.

Stability analysis of self gravitating rings shows that they can be unstable and form clumps (e.g. Dyson 1893; Randers 1942; Wong 1974; Theys & Spiegel 1977). Thus the presence of blobs in the outer ring reflects the relatively high density in it, in good agreement with the fact that roughly 66% of the total H I mass is around the outer optical ring, at a radius of $\simeq 5.6$ kpc. Following the simple arguments of Theys & Spiegel (1977) we see that the number of Jean's lengths around the ring is equal to r/s, where r is the ring radius and s is the radius of the ring cross section. Since r is roughly $72''$ and s roughly $8''$ we find that there should exist 9 Jeans scalelengths along the ring, in very good agreement with the fact that we observe 9 blobs along it. We made a similar analysis of the H I density distribution as a function of angle, but it does not contain the $1.46\,\mathrm{rad}^{-1}$ frequency.

We have looked for deviations from circular motions in the H I velocity pattern along the ring by fitting a sine function to this pattern. The difference between the observed velocity field and the sine function gives the deviation from circular motions. Values between $\pm$ 15 $\mathrm{km\,s}^{-1}$ are found, and some of the changes of sign occur at the extrema of the H I density along the outer ring, as expected for selfgravitating blobs.

(c) The inner pseudoring

We Fourier analysed the $B-I$ colour along the inner pseudoring as we did for the outer ring. However the results are not as telling. Using the same simple arguments as above, one would again expect 9 blobs, since the inner pseudoring has a half thickness of about $3''$ and a radius of about $28''$. The power spectrum has a quite distinct peak at $1.46\,\mathrm{rad}^{-1}$, a value in agreement with the number of Jean's wavelengths, but this peak is not the highest one, which corresponds to a broader feature. Non circular motions are here of the order of 20 $\mathrm{km\,s}^{-1}$. Unfortunately an analysis of these residuals as a function of the azimuthal angle along the ring is not possible due to the low angular resolution of the H I data.

(d) The inner ring

In Fig. 1d it can be noticed that the region inside the inner pseudoring is more intense in Hα than the one outside it. Several structures appear in this inner area. There is a blue inner ring which is incomplete, and coincides with a complete and intense Hα ring. It is surrounded by a redder and more complete ring, clearly visible in Fig. 1c. Both the colour and Hα images suggest the presence of two nuclear spiral-like arm features, which extend to the inner pseudoring. Their winding direction is the same as that of the outer flocculent arms (Fig. 1a) and they are both located in the southern part of the galaxy. One of them is much more evident than the other, and can also be seen in the Hα picture. Finally the central bluer zone corresponds to the LINER nature of NGC 7217, and is almost certainly a zone containing a burst of star formation.

5. Concluding remarks

From our combined photometric and kinematical data on NGC 7217, we find a consistency between the location of the observed rings and resonances due to a bi-symmetric pattern. Intense star formation is going on in the rings, and the outer ring, very strong in H I, is perhaps breaking up due to self-gravity effects. However, in our data, we cannot identify clearly the feature responsible for setting up this pattern. Though the rings remind us that the galaxy could be a barred spiral, the absence of an identifiable oval in the I-image argues against this. Either a weak oval can be found in e.g. K-band images, or the bar has decayed while the ring structure still survives.

Acknowledgements. LV-M acknowledges the hospitality and financial support of the Observatoire de Marseille, where most of this work was carried out. We thank I. Márquez and Dr. M. Moles allowing us to use optical rotation data of NGC 7217, and Dr. Richard Pogge for the Hα image of this galaxy. LV-M acknowledges helpful discussions with Dr. R. Garrido, Dr. A. del Olmo, Dr. M. Moles, I. Márquez, Dr. J. Masegosa and Dr. J. Perea.

References

Athanassoula E., Bosma A., Crézé M., Schwarz M.P., 1982, A&A 107, 101
Athanassoula E., Bosma A., Papaioannou S., 1987, A&A 179, 23
Begeman K., 1987, Ph. D. thesis, University of Groningen
Bos A., Raimond E., van Someren Greve H.W., 1981, A&A 98, 251
Burstein D., Heiles C., 1984, ApJS 54, 33
Buta R., 1986, ApJS 61, 631
Buta R., Crocker D.A., 1991, AJ 102, 1715
de Vaucouleurs G., Buta R., 1980, AJ 85, 637
de Vaucouleurs G., de Vaucouleurs A., Corwin H.G. et al., 1991, Third Reference Catalogue of Bright Galaxies. Springer, Berlin
Dyson F.W., 1893, Philos. Trans. R. Soc. London Ser. A 184, 1041
Gallagaher J.S. III, Hunter D.A., Tutukov A.U., 1984, ApJ 284, 544
Högbom J.A., Brouw W.N., 1974, A&A 33, 289
Keel W.C., 1983, ApJ 268, 632
Kennicutt R.C., 1983, ApJ 272, 54
Kennicutt R.C., Kent S.M., 1983, AJ 88, 1094

Peterson C.J., Rubin V.C., Ford W.K., Roberts M.S., 1978, ApJ 226, 770
Pierce M.J., Tully R.B., 1992, ApJ 387, 47
Pogge R.W., 1989, ApJS 71, 433
Randers G., 1942, ApJ 95, 88
Sandage A., 1961, The Hubble Atlas of Galaxies. Carnegie Inst. of Washington
Schwarz M.P., 1981, ApJ 247, 77
Schwarz M.P., 1984a, A&A 133, 222
Schwarz M.P., 1984b, MNRAS, 209, 93
Schwarz M.P., 1984c, Proc. Astr. Soc. Australia, 5, 464
Schwarz M.P., 1985, MNRAS, 212, 677
Savage B.D., Mathis J.S., 1979, ARA&A 17, 73
Theys J.C, Spiegel, E.A., 1977, ApJ 212, 616
Tully R.B., 1988, Nearby Galaxies Catalog, Cambridge Univ. Press, Cambridge
Verter F., 1987, ApJS 65, 555
Wong C., 1974, ApJ 190, 675
Young J.S., Knezeck P.M., 1989, ApJ 347, L55